Available online at www.sciencedirect.com
ScienceDirect
Journal of the European Ceramic Society 27 (2007) 1493–1502
www.elsevier.com/locate/jeurceramsoc

Manufacturing and performance testing of sol/gel based oxidation protection systems for re-usable space vehicles

V. Liedtke *, I. Huertas Olivares, M. Langer, Y.F. Haruvy

ARCS (ARC Seibersdorf Research GmbH), Austria

Available online 15 June 2006

Abstract

Future re-usable spacecraft replacing the US Space Shuttle could be manufactured with heat shields made of carbon fibre reinforced materials; most likely using carbon fibre reinforced silicon carbide (C/SiC). These materials combine excellent thermo-mechanical properties, low weight, and high strength. They can be manufactured by various established production processes. The main drawback is the sensitivity of the carbon fibre against oxidation. An oxidation protection system is required to avoid carbon fibre burn-off during the re-entry phase, where temperatures higher than 1550 °C are reached.

Most of the oxidation protection systems currently available are manufactured by costly and time-consuming multilayer chemical vapour deposition (CVD) processes. In this work, novel sol/gel based SiC coatings have been developed and tested under approximately identical re-entry conditions (mechanical, thermal, and chemical loads).

The manufacturing and application process of several sol/gel based oxidation protection systems are presented, as well as the characterisation of the materials and the post mortem micro structural analysis after various re-entry test conditions.

The results show that the oxidation protection performance is comparable to the oxidation protection systems currently available on the market, however, at significantly lower manufacturing costs.

Keywords: Sol/gel processes; Composites; Lifetime; SiC; Protective coatings

1. Introduction

1.1. Background and rationale for the study

For manned spaceflights, only single-use vehicles of the Russian Soyuz and the Chinese Shenzhou type are currently available. The US Space Shuttle is planned to resume operations within this year, but – even if this is being accomplished – the deadweight/payload ratio of this design originating from the 1970s will hardly make it a commercially attractive alternative.

The key feature for future multiple-mission spacecrafts is the design of the heat shields that are required not only to ensure reliable and failure-tolerant thermal protection, but must also be structural elements for significant deadweight reduction compared to the Space Shuttle. Carbon-fibre reinforced ceramics provide the optimal performance-to-weight ratio. C/SiC is nowadays the most promising and most frequently utilized composite material for highly demanding thermo-mechanical performance in space missions, i.e. for reusable heat-shields and heat-exposed elements. This family of CMC materials was extensively studied in the last decade.[1–4] C/SiC components fabricated with high-strength carbon fibres components are of particular interest for these studies, since they provide the best strength and stiffness performance at temperatures as high as 2000 °C. It was however clear that thermally loaded C/SiC components require an external oxidation protection system (OPS) to prevent carbon-fibres oxidation during re-entry, and progressive CMC degradation thereafter.

1.2. Current types of OPS

The fabrication of suitable OPS can be achieved by different routes. The simplest CVD-based OPS is a CVD-SiC; this already provides sufficient protection at temperatures above 1000 °C, but due to shrinkage cracks at lower temperatures, the protection in the temperature range from 450 to 1000 °C is insufficient. Commercially applied CVD-based OPS therefore comprise of

* Corresponding author at: ARC Seibersdorf Research GmbH, Aerospace Materials Technology, A-2444 Seibersdorf, Austria.
Tel.: +43 50550 3346; fax: +43 50550 3366.
E-mail address: volker.liedtke@arcs.ac.at (V. Liedtke).

0955-2219/$ – see front matter © 2006 Elsevier Ltd. All rights reserved.
doi:10.1016/j.jeurceramsoc.2006.05.052

one or more SiC-layers, and several functional layers to ensure a sufficient protection over the entire temperature range from approximately 450 to more than 1600 °C. Additionally, the functional layers shall provide self-healing or crack-sealing ability of the OPS, typically by formation of glassy phases with oxygen. Their common failure mode is either cracking or spallation of the OPS, and subsequent oxidation of the CMC.

Slurry-type coatings comprise a binder and a high melting powder, e.g. various carbides, oxides, nitrides, silicides, and the like. They are applied at RT and thermally cured to form a dense layer on the substrate. As with CVD-coatings, multi-layer systems are commonly used, and functional layers are employed. Their main failure mode is evaporation and thinning of the OPS after prolonged exposure to high temperatures.

Sol/gel based systems can be regarded as an improved slurry technology, where the binder is reacting into part of the final coating. Multi-layer systems are commonly used. Until recently, the main drawback of these systems was the limited layer thickness of only a few micrometers, requiring a commercially unattractive number of coating steps to ensure reliable protection. This shortcoming could potentially be solved by utilisation of the "fast sol/gel" process, allowing layer thickness of tens of micrometers up to a few 100 μm in one coating step.

Summarising the aforesaid, the OPS currently employed are multi-layered self-healing materials. These OPS exhibit satisfactory performance upon testing. Nonetheless, they present a twofold drawback: (a) the grave fabrication complexity, and its consequent cost impact, and (b) the thermal gradients across the multi-layer coatings, and their consequent grave thermal stresses.

1.3. Application-relevant testing of OPS

The critical testing challenge is to properly test CMC-OPS components under thermo-mechanical re-entry relevant loads, and assess their durability, sustained performance, and reliable reusability. The complexity of loads during a re-entry is difficult to achieve in a single test rig; typically, plasma windtunnels reflect the chemical and thermal loads very well, however are usually not equipped with a dynamic mechanical loading system. Their additional drawback is the severe cost impact on typically very limited project budgets.

The re-entry chamber developed at ARCS combines an up-to-date mechanical loading system and a powerful induction heating system, but plasma effects on the coating cannot be represented. Test costs are significantly lower compared to plasma windtunnels, thus allowing screening tests at reasonable costs; typical costs for a single plasma test cycle is 1000€, and for 100 re-entry cycles (continuous fully-automated operation without changing/inspection of samples in between) can be estimated with 2000–5000€, depending on user-specific specs. A test sequence with 20 cycles, with inspection of samples after each five cycles, typically ranges from 2000 to 3000€.

The current paper describes the OLCHOS testing project carried out at the ARCS. As an "all-in-one" test rig that fulfils all technical and cost-related specifications seems not to be available at all, screening tests have been performed at ARCS under re-entry-relevant conditions (temperature, temperature gradient, and gas pressure), and results were then verified by plasma testing on a limited number of samples.

The performance of the OPS is discussed, in correlation with the various thermo-mechanical regimes, and their incurred degradation features. Further, plasma test-results of the most promising OPS are discussed in the context of possible active oxidation. The comprehensiveness of this ensemble of tests is further assessed, and its relevancy to oxidation durability, functional reliability and overall reusability of the OPS-CMC systems during re-entry missions, as also shown in.[6] Finally, a trade-off assessment is described, of the OPS performance versus practical limitations, to select three OPS for technology demonstrator samples.

2. Experimental

2.1. CMC base materials

Two different CMC base materials, qualified for space applications, have been evaluated in the present study. EADS base material has been manufactured by a liquid phase infiltration (LPI) process. Its ultimate tensile strength at RT is 140 MPa, with a Young's modulus of 17.6 GPa and a strain-to-failure of approx. 0.6%. MAN base material, manufactured by a physical vapour infiltration (PVI) process, exhibits a RT UTS of 420 MPa, a Young's modulus of 44.1 GPa and a strain-to-failure of approx. 0.9%.

2.2. Oxidation protection systems

Before applying the sol/gel based OPS, to ensure good adhesion to the base material, a CVD-SiC layer of approx. 30 μm has been applied on the MAN base material, and a layer of approx. 60 μm on the EADS base material.

The chemistry of the fast sol/gel process has been described in detail in Ref.[5] A monomer composition of 90% methyl-trimethoxy-silane (MTMS) and 10% dimethyl-dimethoxysilane (DMDMS) has been reacted under acid catalysis.

For OPS 7, 30 wt.% of fine alumina powder (ALCOA A 1656, particle size approx. 0.5 μm) have been added. A layer of this sol was brushed onto the composite, and after drying in a furnace at 80 °C for 12 h, the coating was then thermally converted at a maximum temperature below 1000 °C. After this treatment, the layer thickness was found to be approx. 150 μm. This coating procedure was repeated once, followed by a cover layer of pure sol/gel, i.e. without alumina powder addition.

For OPS 8, partly stabilised zirconia powder (TOSOH TZ-8Y, grain size approx. 0.1 μm) has been used instead, and three layers of this system have been applied.

OPS 9 is similar to OPS 7, but the third layer consists of alumina-enhanced coating rather than pure sol/gel.

To assess the performance of these novel coatings in direct comparison with established systems, three coatings made with three to seven layers of CVD- and slurry coatings were applied

on the EADS base material; these OPS are designated OPS 1–3. Three more coatings were applied only onto MAN base material, where OPS 4 is a pure CVD system, and OPS 5 and 6 are multilayer systems of CVD- and slurry coatings.

2.3. Testing and diagnostics non-destructive and micro-structural diagnostics

Sonography: a panametrics MULTISCAN system was employed to inspect (a) pristine samples, as QA before testing, and (b) post-test samples exhibiting significant degradation, as a complimentary data source. Samples were submerged in deionized water, employing a 2.25 MHz transducer. The number of TPS inspected before the re-entry test has been limited, to avoid possible damage to some OPS that might be sensitive to water.

For inspection of the samples before and after impacting, an air coupling system has been employed at ILK Dresden. Technical specifications are available in the open literature.

SEM/EDAX (Zeiss DSM 950/Gruen SAAS 2000) system, facilitating 15×–200k×, was employed for comparative analysis of the pristine versus tested micro-structural features of the test coupons, and for assessing OPS adhesion after tests.

Inverse light metallographic microscope (Reichert-Jung MeF3, 16×–1600×) was employed for sample inspection after exposure to re-entry conditions, and for digital picture acquisition of significant findings.

2.4. Mechanical properties

Room temperature tensile strength was tested with a universal testing machine (Shimadzu AGC-10/TC). Ultimate tensile strength (UTS) and residual tensile strength (RTS) were tested per DIN EN 658-1, employing type-3 samples. Test conditions: ambient air and temperature; crosshead speed 2 mm/min; strain data recording by videotape (Sandner ME46 Extensometer).

Impact durability: these testings were subcontracted to Technical University Dresden, ILK unit (Institut fuer Leichtbau und Kunststofftechnik). The impact energy was tuned to 0.74 J at 1.3 m/s impact speed to produce a visible damage to the OPS yet an insignificant damage to the bulk material. The objective of this test was to assess the real-life survivability of the OPS under assembling-disassembling relevant conditions.

2.5. Thermo-mechanical testing under re-entry conditions

Set-up: the ARCS-built re-entry simulation chamber was employed to subject the materials being tested to the mechanical, thermal, and atmospheric loads typical of the re-entry phase of a space mission. Its inductive heating unit, capable of >−223 °C/s, >1800 °C, is operated via pyrometers and PID controller. The servo-hydraulic dynamic test machine of the simulator, LF 70S (Walter and Bai), facilitates dynamic loads of up to 70 kN with a frequency of up to 70 Hz. Two micro-computers served for system control and data logging.

Mechanical loads: mean load levels were 20% and 50% of the RT UTS, of each base material (see Section 3.2). Superposed dynamic loading was 5 Hz sinusoidal, with amplitude of ±2% and ±5% of the RT UTS, at 20% and 50% mean load, respectively.

Thermal regime: heating and cooling profiles were taken from several re-entry vehicle design projects[3,4] and can be regarded as representative for the re-entry trajectory of a manned re-usable vehicle. Heating rate from 350 to 1450 °C (1550 °C, respectively) was 4 °C/s, dwell time at max. temperature 5 min, cooling to 750 °C with 3.5 °C/s, then to 550 °C with 3.3 °C/s, and finally to 350 °C with 2.5 °C/min.

Because of the applied cold grippings, the maximum temperatures as shown above are only reached in the centre of the specimens. At the ends, their temperature was always below 200 °C, thus inducing severe thermal gradients into the sample. The shape of the temperature distribution along the sample axis resembles the profile of a Gauss curve. This reflects the thermal gradients expected for structural elements such as leading edges or body flap, but to a higher extent than in real structures.

Cycles orchestration: the number of mechanical cycles was set proportional to the number of thermal cycles. The mean load was superposed a dynamic sinusoidal load of 5 Hz, with an amplitude of ±10% of the respective mean load. Thus, 100 thermal cycles at 1450 and 1550 °C, correspond to 465,000 and 477,500 mechanical cycles, respectively, with additional <1% cycles during sample installation and test initiation.

Atmosphere regime: for simplification and significant reduction of cycle time, tests were performed at a constant pressure. A 40 mbar were applied for most of the thermo-mechanical tests. A few tests were carried out at 80 mbar and 1 bar. At all pressures, ambient air was streaming through the test chamber at a rate of 20 ± 1 N l/h.

Test termination criteria: sample break was the sole termination criterion for all tests, since "softening" or elongation could not be reliably detected.

2.6. Plasma testing

Plasma tests were performed in the L2K facility of DLR in Cologne, Germany, under two different plasma streaming conditions in order to achieve two different temperature levels. Relevant test parameters are compiled in Table 1.

These parameters were selected in such a way that sample surface temperature should reach 1450 °C for flow condition (FC) I, and 1550 °C for FC II. Calibration was done with OPS 2 samples.

Due to facility's load limit (2500 N), a load equivalent to only 5% of the ultimate tensile strength was employed. Such a load eliminated premature sample failure, but portrayed some mechanical pre-loading, similar to real-case scenarios of a vehicle upon re-entry. Thus, loads of 500 and 1500 N were employed for the EADS and MAN base materials, respectively.

Each sample was tested for three cycles at the respective flow condition. After each cycle, sample mass was recorded.

Table 1
L2K parameter sets for flow conditions I and II

Flow conditions	FC-I	FC-II
Air mass flow rate (g/s)	55	75
Reservoir pressure (hPa)	1640	2200
Total temperature (°C)	5100	4980
Specific enthalpy (MJ/kg)	9.7	9.3
Nozzle throat/exit diameter (mm)	29/100	29/100
Model location	368	318
Free stream Mach number (mm)	5.6	5.4
Free stream velocity (m/s)	3177	3123
Free stream pressure (hPa)	1.9	3.0
Free stream temperature (°C)	914	679
Free stream density (kg/m^3)	8.5E−04	1.3E−03
Mole fraction of O_2	0.009	0.019
Mole fraction of N_2	0.646	0.651
Mole fraction of O	0.324	0.303
Mole fraction of N	<10E−06	<10E−06
Mole fraction of NO	0.020	0.027

3. Results, observations and discussion

3.1. Room temperature tensile tests

Tensile strength and Young's modulus data for the various CMC-OPS systems at room temperature is displayed in Table 2. These data provide the baseline mechanical properties necessary for properly planning the load levels during the thermo-mechanical tests. Uncoated base materials have not been tested; EADS base material was tested with OPS 1–3 (labelled EE-C1, EE-C2, and EE-C3), while MAN base material was tested with OPS 4 and 5 (MM-C4 and MM-C5).

The significant difference between the two CMC base materials is evident, but the type of OPS applied does not have a relevant influence on the UTS; these differences are within the scatter band of test results.

The UTS of the MM samples are lower limits data. This is due to difficult gripping that should be sufficiently strong to avoid slipping, yet sufficiently tender to avoid OPS damage. Nevertheless, the <20% incurred inaccuracy is practically insignificant in the context of the thermo-mechanical durability assessment.

Table 2
Room temperature tensile test results

Base material	Coating	Tensile strength (MPa)	Young's modulus (GPa)
EADS	C1	136.5	18.18
EADS	C2	140.5	18.37
EADS	C3	141.8	17.58
EADS	Mean value	139.6	18.04
MAN	C4	431.1	46.03
MAN	C5	410.8	42.13
MAN	Mean value	421.0	44.08

3.2. Thermo-mechanical tests

Load levels: loading is crucial for the TMT durability assessment, since strains induced thereby in the OPS causing cracks broadening and oxidative degradation of the CMC thereafter. In the thermo-mechanical tests, two different load levels were applied for each CMC-OPS system. As the RT UTS of both base materials differs significantly, 20% and 50% of the respective RT UTS were selected, with most tests performed at 20% RT UTS. Such load level is accepted as a typical loading applicable for large areas of re-entry structures. Practically, apart from joints and hinges, only few parts of the heat shield are actually loaded significantly above 20% RT UTS.

Temperature: most tests were performed at 1450 °C. Additionally tests at 1550 °C to assess the thermal limits of the OPS were carried out.

To better focus on the OPS performance rather than the base materials and their inherent differences, the results are displayed separately for each base material. It should be mentioned, however, that for re-entry applications, the entire OPS-CMC system needs to survive the TMT loads and, hence, the overall performance of these systems is the primary interest.

3.3. EADS base material

3.3.1. Standard test condition: 1450 °C T_{max}, 20% UTS

Mass change and RTS of EADS-based CMC-OPS performed at T_{max} of 1450 °C and load level of 20% RT UTS are presented in the following Table 3. All specimens survived the envisaged 100 thermo-mechanical cycles. The <0.2% insignificant mass changes after 100 cycles are in accord with the finding that all the samples retained ca. 80–90% of their original strength, indicating insignificant degradation during tests. Sol/gel based OPS 7–9 perform identical to the established OPS 1–3.

3.3.2. Test condition II: increasing the load level to 50% UTS

Upon raising the load level to 50% RT UTS, tests result in a substantial increase of the mass loss, as shown in Table 4. Under this increased load, none of the samples survived 100 cycles. This finding obviously manifests a graver OPS damage under the increased load, probably because the load-induced higher strain of the CMC exceeds the OPS flexibility limits, causing

Table 3
Cycles survived, mass change, and residual strength of EADS base samples tested at 1450 °C/20% UTS

OPS base material	Cycles survived	$\Delta m/m_0$ (%)	Residual strength	
			(kN)	RT (%)
1, EADS	100	−0.07	8.01	78.9
2, EADS	100	0.04	8.31	80.1
3, EADS	100	0.09	9.94	93.4
7, EADS	100	−0.06	9.60	91.0
8, EADS	100	−0.04	9.08	86.1
9, EADS	100	−0.20	8.57	81.2

Table 4
Cycles survived, mass change, and residual strength of EADS base samples tested at 1450 °C/50% UTS

OPS base material	Cycles survived	$\Delta m/m_0$ (%)	Residual strength	
			(kN)	RT (%)
1, EADS	38	−1.22	n/a	n/a
2, EADS	35	−0.29	n/a	n/a
3, EADS	44	0.15	n/a	n/a
7, EADS	38	−1.03	n/a	n/a
8, EADS	45	−0.61	n/a	n/a
9, EADS	32	−0.92	n/a	n/a

Table 6
Cycles survived, mass change, and residual strength of EADS base samples tested at 1550 °C/20% UTS

OPS base material	Cycles survived	$\Delta m/m_0$ (%)	Residual strength	
			(kN)	RT (%)
1, EADS	100	−0.02	8.62	84.8
2, EADS	100	0.14	8.78	84.6
3, EADS	100	0.06	9.24	86.8
7, EADS	100	−0.07	8.15	77.2
8, EADS	100	−0.47	6.80	64.4
9, EADS	100	−1.02	5.71	54.1

cracks to open and making way for oxygen that destroys the carbon fibre reinforcements.

Comparing sol/gel based OPS 7–9 to the other systems, there is again no difference in performance.

3.3.3. Test condition III: the effect of impact-damage to the OPS

For this test, impact damaged samples have been employed. The increased mass loss compared to standard test conditions clearly indicates a significant impact-produced damage to the OPS and the CMC thereafter.

Except for OPS 9, all specimens survived the 100 cycles; their RTS is however significantly lower compared to not impact damaged ones, as shown in Table 5. As for the mass loss, a significant reduction in RTS compared to non-impacted samples or – for OPS 9 – a premature failure of the specimen indicates a damaging of the OPS and a subsequent oxidative degradation of reinforcing carbon fibres.

Under these conditions, the sol/gel based OPS 8 and 9 show a reduced performance compared to the other systems; OPS 7 performs better, but still not as good as the best competitors.

3.3.4. Test condition IV: increasing the temperature to 1550 °C

The −173 °C increase in the temperature reflects a requirement for thermally more demanding re-entry trajectories. It has to be ensured that the TPS are not already at their thermal performance limits, as a sufficient safety margin must be available. All specimens survived 100 cycles; mass change and RTS are shown in the following Table 6.

Compared to testing at 1450 °C, the mass changes are higher. For OPS 2, a significant mass gain has been observed, while OPS 8 and 9 already exhibit relatively high mass losses. Though these mass changes are comparable to those found for impact-damaged samples (see Table 5), the RTS is retained to a higher degree.

Microscopic analysis of the OPS after tests reveals a significant reduction in the thickness for sol/gel based OPS 8 and 9 in the hottest zone, though the inner layer is still intact and ensures protection of the CMC structure.

Compared to OPS 1–3, the sol/gel based OPS seem to be closer to their thermal limits; the performance is already being slightly reduced, but can still be regarded as sufficient.

3.4. MAN base material

3.4.1. Standard test condition: 1450 °C T_{max}, 20% UTS

Test results for MAN based specimens following the thermo-mechanical tests, with cycling T_{max} of 1450 °C and 20% RT UTS, are shown in Table 7.

The mass loss of several samples ruptured before 100 cycles is extremely high. This is partly because of large amounts of debris released by MAN based samples, partly because of severe oxidative degradation of the specimens.

The low RTS of sol/gel based OPS 8 is in good correlation with the high mass loss of the sample, though also the OPS 5 with a mass gain of more than 0.8% retains only 60% of its initial strength, indicating some damage to the structure. All other samples failed before the envisaged 100 cycles had been completed.

Table 5
Cycles survived, mass change, and residual strength of EADS base samples with impact-damaged OPS tested at 1450 °C/20% UTS

OPS base material	Cycles survived	(%)	Residual strength	
			(kN)	RT (%)
1, EADS	100	−0.55	4.74	46.7
2, EADS	100	−0.47	3.65	35.2
3, EADS	100	−0.24	5.38	50.5
7, EADS	100	−0.56	3.37	31.9
8, EADS	100	−1.4	0.10	0.9
9, EADS	86	−0.96	n/a	n/a

Table 7
Cycles survived, mass change, and residual strength of MAN base samples tested at 1450 °C/20% UTS

OPS base material	Cycles survived	$\Delta m/m_0$ (%)	Residual strength	
			(kN)	RT (%)
4, MAN	43	−2.13	n/a	n/a
5, MAN	100	0.82	19.20	60.3
6, MAN	84	−4.01	n/a	n/a
7, MAN	63	−1.82	n/a	n/a
8, MAN	100	−1.42	8.71	27.4
9, MAN	94	−2.25	n/a	n/a

Table 8
Cycles survived, mass change, and residual strength of MAN base samples tested at 1450 °C/50% UTS

OPS base material	Cycles survived	$\Delta m/m_0$ (%)	Residual strength	
			(kN)	RT (%)
4, MAN	11	−0.44	n/a	n/a
5, MAN	27	−0.76	n/a	n/a
6, MAN	7	−3.41	n/a	n/a
7, MAN	7	−1.48	n/a	n/a
8, MAN	7	−1.19	n/a	n/a
9, MAN	5	−0.78	n/a	n/a

Though partly not surviving 100 cycles, sol/gel based OPS perform comparable to the competitor systems. The generally lower number of cycles survived has to be attributed to the base material performance.

3.4.2. Test condition II: increasing the load level to 50% UTS

As already described for the EADS base material, the increased load level did reduce the lifetime of the specimens significantly; and none of the systems survived only 30 cycles. Their mass loss at the test end-point was less than 3.5%, indicating that the primary damage affected the carbon fibre reinforcement. Results are compiled in the following Table 8.

Apart from the slightly better performance of OPS 5, all systems show only poor lifetime, irrespective of the way the OPS were applied.

3.4.3. Test condition III: the effect of impact-damage

As presented in Table 9, only the specimen coated with OPS 5 did survive the full 100 cycles, though the mass loss and the RTS already indicate a significant structural damage. All other systems failed prematurely, indicating that impact damage does reduce the lifetime of MAN based samples more than for EADS based ones.

Sol/gel based OPS do not perform sufficiently under these conditions.

3.4.4. Test condition IV: increasing the temperature to 1550 °C

Increasing the T_{max} to 1550 °C also resulted in an accelerated damage to all of the samples, and none survived the full 100 cycles. As shown in Table 10, OPS 5 again shows the longest lifetime. The sol/gel based OPS perform as good as or better than the other two systems OPS 4 and 6.

Table 9
Cycles survived, mass change, and residual strength of MAN base samples with impact-damaged OPS tested at 1450 °C/20% UTS

OPS base material	Cycles survived	$\Delta m/m_0$ (%)	Residual strength	
			(kN)	RT (%)
4, MAN	40	−1.2	n/a	n/a
5, MAN	100	−0.59	13.40	42.1
6, MAN	69	−3.79	n/a	n/a
7, MAN	47	−2.22	n/a	n/a
8, MAN	39	−1.76	n/a	n/a
9, MAN	37	−1.46	n/a	n/a

Table 10
Cycles survived, mass change, and residual strength of MAN base samples tested at 1450 °C/50% UTS

OPS base material	Cycles survived	$\Delta m/m_0$ (%)	Residual strength	
			(kN)	RT (%)
4, MAN	27	−1.06	n/a	n/a
5, MAN	76	−2.74	n/a	n/a
6, MAN	41	−4.34	n/a	n/a
7, MAN	53	−3.12	n/a	n/a
8, MAN	38	−2.39	n/a	n/a
9, MAN	57	−2.59	n/a	n/a

3.5. Oxygen pressure effect during thermo-mechanical tests

For completion of assessment of damage parameters, tests have been performed not only under 40 mbar pressure, but also at 80 and 1000 mbar of ambient air, with exchange rate of 36 N l/h like before. The data of mass changes and residual strength, versus oxygen pressure, following the thermo-mechanical tests are displayed in Table 11.

The salient indication from these results it that between 40 and 80 mbar the oxygen pressure effect is insignificant: The changes in both the mass and UTS are well within the scale of scattering. At the ambient pressure, however, the mass, UTS and cycles survival decrease drastically. Though the ambient pressure testing seems highly effective for fast screening CMC/OPS systems, its relevancy to re-entry applications is highly questionable.

3.6. Plasma tests

The actual surface temperatures for several OPS differed significantly from the predictions, and additionally, temperatures at the beginning and at the end of the isothermal dwell time were also not the same. Surface temperatures of plasma test samples are presented in the following Table 12.

The reason for these temperature discrepancies may be explained with different surface emittances of the respective coatings, though an error calculation indicates that this error should not exceed 40 °C. It was therefore assumed that the enthalpy of the plasma jet could not be distributed from the surface into the bulk sufficiently. This may either be caused by very low thermal diffusivity of the OPS, or spallation of coating layers. Subsequent investigations are foreseen to clarify this important finding.

Mass loss during and RTS after plasma tests are compiled in the following Table 13.

All specimens (except with OPS 3 and 4) survived the three test cycles without indication for relevant structural damage, with insignificant differences between the two flow regimes utilized. RTS ranging from 90% to 110% of the initial RT UTS can be regarded as within the scatter band of such materials,

Table 11
Results of tests at different pressures; Test conditions: 1450 °C/20% UTS

Base material	OPS	Sample designation	Pressure (mbar)	Cycles survived	$\Delta m/m_0$ (%)	RTS	
						(kN)	RT (%)
EADS	2	EE-C2.04	40	100	0.04	8.31	80.1
		EE-C2.10	80	100	0.06	7.05	68.0
		EE-C2.11	1000	45	−2.93	n/a	n/a
EADS	3	EE-C3.04	40	100	0.09	9.94	93.4
		EE-C3.12	80	100	0.13	8.81	82.7
MAN	4	MM-C4.04	40	43	−2.13	n/a	n/a
		MM-C4.10	80	46	−1.65	n/a	n/a
		MM-C4.11	1000	18	−2.36	n/a	n/a

Cycles survived, mass change and RTS shown.

Table 12
Surface temperatures of plasma test samples

Sample	Sample surface temperatures								
	End of dwell time (°C)			Maximum (°C)			Difference (°C)		
	First run	Second run	Third run	First run	Second run	Third run	First run	Second run	Third run
EE-C1.07	1479	1462	1460	1479	1470	1470	0	8	10
EE-C3.10	1450	1442	1445	1450	1442	1445	0	0	0
EA-C7.07	1580	1597	1596	1580	1615	1610	0	18	14
EA-C9.07	1551	1487	1492	1600	1600	1635	49	113	143
MM-C4.07	1525	1493	1480	1540	1585	1510	15	92	30
MM-C5.07	1515	1495	1462	1515	1560	1505	0	65	43
MA-C7.08	1481	1500	1512	1585	1620	1600	104	120	88
MA-C9.08	1470	1498	1499	1490	1560	1560	20	62	61
EE-C1.08	1519	1515	1499	1530	1515	1499	11	0	0
EE-C3.11	1512	1518	1523	1535	1518	1523	23	0	0
MM-C4.08	1561	1539	1555	1595	1585	1555	34	46	0
MM-C5.08	1583	1420	1536	1600	1435	1536	17	15	0

Temperature at end of dwell time, maximum, and difference shown. Last four tests under FC-II, all others under FC-I.

Table 13
Mass change after each run and mechanical strength after three plasma test cycles

FC	Sample	Mass change (%)			E (GPa)	R_m (MPa)	RTS (%)
		First run (%)	Second run (%)	Third run (%)			
1	EE-C1.07	0.11	−0.03	0.03	18.94	146.97	105.60
1	EE-C3.10	−0.17	−0.12	−0.19	16.32	133.44	99.90
1	EA-C7.07	−0.32	−0.21	−0.24	17.39	146.24	97.30
1	EA-C9.07	−0.21	−0.15	−0.12	17.74	140.62	93.00
1	MM-C4.07	−0.51	−0.58	−0.61	41.93	321.04	77.30
1	MM-C5.07	−0.38	−0.38	−0.44	40.73	442.03	106.20
1	MA-C7.08	−0.25	−0.38	−0.34	43.08	366.49	87.20
1	MA-C9.08	−0.24	−0.27	−0.27	45.44	422.39	97.00
2	EE-C1.08	−0.15	−0.10	−0.10	18.51	143.83	103.60
2	EE-C3.11	−1.82	−2.26	−2.61	18.16	113.06	78.40
2	MM-C4.08	−0.50	−0.87	−0.87	48.06	358.87	82.20
2	MM-C5.08	−0.60	−0.62	−0.57	24.99	419.31	100.30

as only a single specimen per test condition had been evaluated.

The Young's modulus of MM-C5.08 (MAN base, OPS 8) is faulty due to an error in the strain recording.

Mass loss of EE-C3.11 (EADS base, OPS 3) was caused by spallation of OPS and subsequent damage to the sample.

Summarising the plasma test results, the sol/gel based OPS do not show any indication of active oxidation or other plasma-induced decomposition reactions; their performance under plasma conditions is truly comparable to established systems.

3.7. Sample's inspection and micro-analysis

The crucial features of the OPS are integrity and coherence throughout the mission, to reliably protect the CMC underneath. Therefore, a comprehensive study of the sample's surface before and after the TMT cycles was carried out throughout the project. This diagnosis has provided a valuable insight of the less acknowledged OPS failure modes, namely defect-originated damage mechanisms.

From the results of these inspections, the coating/base material pairings can be subdivided into several groups with similar appearance and failure behaviour:

3.7.1. EADS base material with OPS 1–3

The as-received coatings show a fine surface roughness with a grid of narrow shrinkage cracks. After exposure to oxygen at elevated temperatures, the formation of fine crystallites of silica or quartz can be detected on the surface.

Composites tested at 1450 °C/50% UTS fail due to delamination or spallation of the entire coating. This can be attributed to the high strain of the bulk material under the mechanical load, exceeding the flexibility of the OPS.

Under all other thermo-mechanical test conditions applied within this project, these coatings are not severely degraded. At 1550 °C, the outer layer of the coating begins to melt.

At elevated temperature, the cracks in the coating are mainly filled with a light amorphous phase, indicating self-healing capacities. Finally, plasma conditions cause colour changes, mainly at the backside, but do not affect the coating significantly.

3.7.2. MAN base material with OPS 4–6

The surface of these OPS shows a smooth structure and a brownish colour. At elevated temperatures under oxygen, a colour change to dark was observed. For OPS 6, large bubbles formed at temperatures exceeding approximately 500 °C. These bubbles seem to reduce the integrity of the underlying layers of the OPS.

All coatings tend to be thermally degraded at the hottest zones of the composites, thus resulting in sample fracture in the middle zone. At 1550 °C, the top layer of the OPS seems to be partly molten. After exposure to elevated temperatures, cracks can be observed that are filled with a light amorphous phase, indicating self-healing capacities. On the surface, crystallines are being formed that resemble silica or quartz.

Under plasma conditions, the top layers of the OPS seem to change the structure completely or to disappear at the back side. At the front side, the top layers look similar to those after thermo-mechanical tests.

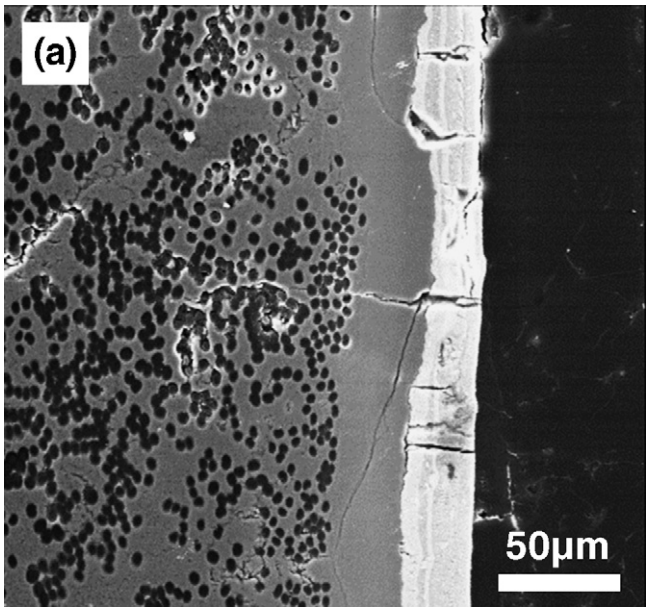

Fig. 1. (a) Position from edge (mm): 75 (fracture zone).

3.7.3. EADS base material with sol/gel based OPS 7–9

The appearance of the as received coatings is less uniform than for coatings that were discussed above. Additionally, some samples show severe shrinkage cracks after manufacturing, while other specimen with the same OPS seem to be crack-free. The uniformity of the OPS application process will require some further improvement to ensure quality consistency.

Thermal treatment leads to a colour change to dark for most of the specimen. During thermal treatment, cracks tend to close and are – at least partly – filled with a light amorphous phase, indicating at least limited self-healing abilities. The formation of quartz crystals can be observed for most of the specimen. In the centre, the top layer of the OPS tends to be reduced in thickness, indicating thermal degradation effects.

Under plasma conditions, these OPS tend to change colour and exhibit cracks. Changes are comparable to those after thermo-mechanical tests.

Details of coating OPS8 (1450 °C/50%UTS) is shown in Fig. 1: (a) position from edge (mm): 75 (fracture zone); damage at interface between inner and middle layer more pronounced. Shrinkage cracks in the inner layer continue both into outer layers and into bulk material. Fig. 2: (b) position from edge (mm): 90; outer layer partly disappeared. Many cracks in outer layer, but stopped at interface to second layer. Formation of bubbles starts in outer layers of OPS. Fig. 3: (c) position from edge (mm): 115 (centre): few small areas of outer layers not well adhering to inner layer. Outer layers no longer distinguishable, formation of small bubbles of some micrometers diameter.

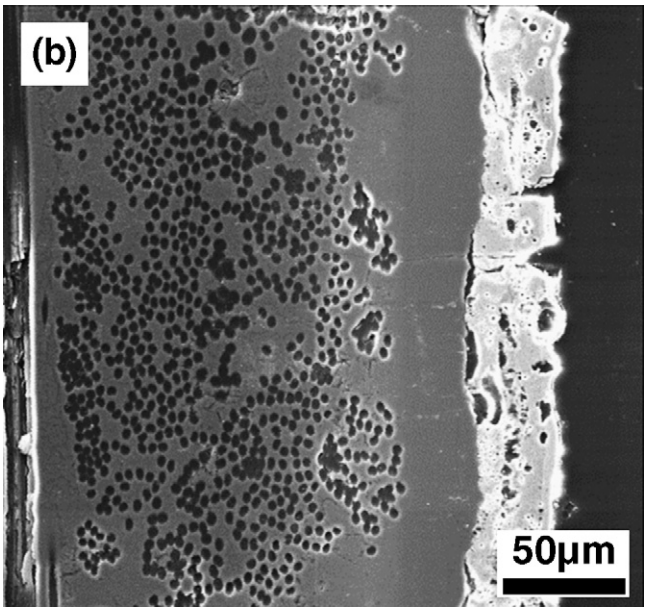

Fig. 2. (b) Position from edge (mm): 90.

3.7.4. MAN base material with sol/gel based OPS 7–9

For OPS 7 and 8, shrinkage cracks can be observed after OPS application. When subject to moderate thermal loads, these cracks tend to be filled, but re-appear in the hottest central zones of the specimen.

A colour change during thermal treatment can be observed, as already described for EADS base material with these OPS. The thickness of the outer OPS layer seems to be slightly reduced in the hottest zone, indicating some thermal degradation. Additionally, the interface of the outer OPS layers to the inner layer and the bulk material requires some improvement.

Under plasma test conditions, these OPS perform similar and show similar degradation effects. OPS 7 show the formation of glassy bubbles at the back side.

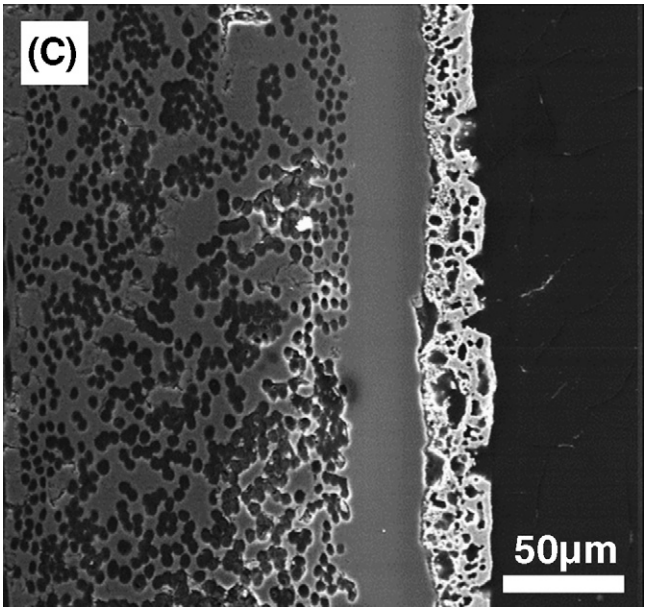

Fig. 3. (c) Position from edge (mm): 115.

3.8. Summary of test results

The OPS performance depends not only on the test conditions (load, temperature, pressure), but also strongly on the base material. This has been demonstrated for ARCS OPS 7–9 that were applied both on EADS and on MAN base materials.

For EADS base material, all OPS investigated showed good protection at 1450 °C and 20% UTS. Increasing the load to 50% caused the failure of all systems at less than 50 cycles. Therefore, no significant differences could be found.

For impacted samples, the performance of the sol/gel-based OPS 8 and 9 is reduced, and the specimens fail before reaching 100 cycles. Also, OPS 7 shows higher mass loss and lower RTS compared to OPS 1–3. It shall, however, be noted that the sol/gel-based OPS were not designed for self-healing ability.

At 1550 °C, the thermal limits of the sol/gel based systems seems to be reached, as the mass loss of OPS 8 and 9 is higher, and the RTS is lower than for the other systems.

Summarising these results, the EADS coatings show generally good performance under all test conditions; however the sol/gel based OPS – mainly OPS 7 – show also comparable performance, except for impact damaged samples.

Regarding MAN based specimens; the lifetime seems generally to be lower. This may be attributed to the relatively higher strain of the samples under the respective load levels. The strain-at-failure for EADS base material is approx. 0.60% and 0.88% for MAN base material. Therefore, the respective strains at 20% UTS are 0.12% for EADS and 0.17% for MAN. The difference may already be sufficient for a premature failure of specimens with MAN base material, though it shall be mentioned that the absolute tensile loads applied differ by a factor of three, in favour of MAN base material.

Under all test conditions, MAN's OPS 5 performed best. The sol/gel based systems were comparable to the other MAN coatings, but did not perform as good as on EADS base material.

4. Conclusions

Results have shown that sol/gel based OPS can be applied onto industrial standard CMCs without lengthy optimisation processes. It could be achieved with a simple, fast, and extremely cost-efficient process. Their performance is, under most test conditions, comparable to more complex, more expensive, and more time-consuming to apply systems.

It has, however, become clear that the impact tolerance or the self-healing ability of these systems requires significant improvements. This issue had not been addressed when the OPS generation applied in this study had been developed. It may therefore be necessary to implement an additional coating layer that allows self-healing of cracks and damages via the widely used approach of a glass former.

The thermal limits of the systems could further be improved, either by optimisation of the type and amount of ceramic powder, or by modification of the monomer composition. Thorough testing of these improved systems however might become time-consuming.

References

1. Dogigli, M., Handrick, K., Bickel, M. and Fröhlich, A., CMC key technologies—background, status, present and future applications. In *Proceedings of the fourth European workshop on hot structures and thermal protection systems for space vehicles*, 2002.
2. Handrick, K., Wildenrotter, K., Lange, H. and Weihs, H., Hot movable CMC structures—entrance to a new world of CMC components. In *Proceedings of the third European Workshop on thermal protection systems*, 1998.
3. Pfeiffer, H. and Dogigli, M., All-ceramic body flap for the X-38, a revolutionary step forward. In *Proceedings of the third European conference on launcher technologies*, 2001, pp. 713–723.
4. Wulz, H.G., *Material characterization of C/SiC and joining of C/SiC by use of metallic fasteners, ARC-W-0046*, 1999.
5. Liedtke, V., Huertas Olivares, I., Langer, M. and Haruvy, Y. F., Sol–gel based carbon/silicon carbide composites. *J. Eur. Ceram. Soc.*, 2006, **27**, 1267–1272.
6. Trabandt, U., Reinbold, G.-F., Esser, B., Koch, D., Knoche, R. and Tumino, G., RLV TPS and hot structure operational cost evaluation after life cycle testing with rain, hail, and low speed impact. In *Proceedings of the fourth international symposium atmospheric reentry vehicles systems*, 2005.